

A Zn-Al-Zr layered double hydroxide/graphene oxide nanocomposite enables rapid photocatalytic removal of kanamycin-resistance bacteria and genes via nano-confinement effects

Miao Yu ^{a,b}, Dawei Liu ^{a,b}, Lichao Wang ^c, Jing Xia ^{d,e}, Jianhui Ren ^{a,b}, Yuqiu Fan ^{a,b}, Xiaofeng Zhu ^{a,b}, Jun Wang ^{a,b}, Kun Xiong ^{a,b,*}

^a State Key Laboratory of Environment-friendly Energy Materials, Southwest University of Science and Technology, Mianyang, Sichuan 621010, China

^b School of Materials and Chemistry, Southwest University of Science and Technology, Mianyang, Sichuan 621010, China

^c School of Life Science and Engineering, Southwest University of Science and Technology, Mianyang, Sichuan 621010, China

^d College of Veterinary Medicine, Sichuan Agricultural University, Chengdu, Sichuan 611130, China

^e Key Laboratory of Agricultural Bioinformatics, Ministry of Education, Sichuan Agricultural University, Chengdu, Sichuan 611130, China



ARTICLE INFO

Keywords:

Nano-confinement Effects
Antibiotic-resistance
Photocatalysis
Differential Proteomics
Wastewater Treatment

ABSTRACT

For efficient removal of the antibiotic-resistance bacteria and antibiotic-resistance genes, zirconium-doped zinc-aluminum layered double hydroxide/graphene oxide (Zn-Al-Zr LDHs/GO) nanocomposite has been developed. The Zn-Al-Zr LDHs/GO shows outstanding photocatalytic sterilization, inactivating kanamycin-resistance *E. coli* ($6.53 \log_{10}$ CFU/mL) under the full-wavelength light irradiation within 50 minutes. Owing to the $\cdot\text{O}_2$ formation, it greatly disrupts the respiratory chain of the kanamycin-resistance *E. coli*, thereby leading to a declined yield of adenosine triphosphate, down-regulated expressions of the DNA ligase and polymerase proteins, as well as completely inhibited expressions of the DNA repair proteins. Meanwhile, the strong adsorption capability of the Zn-Al-Zr LDHs/GO towards phosphorus endows it with special nano-confinement effects for ARGs. It results in significantly enriched local concentration of the kanamycin-resistance genes on the Zn-Al-Zr LDHs/GO, consequently enhanced removal ability towards the kanamycin-resistance genes ($4.70 \log_{10}$ copies/mL in 3 hours). This work provides a new strategy for effectively removing the ARB and ARGs.

1. Introduction

With the massive use of antibiotics in the medicine, aquaculture, agriculture and livestock, the inappropriate disposal and discharge of antibiotics have inevitably led to their severe diffusion among the pedosphere and hydrosphere [1–3]. The sub-lethal concentrations of antibiotics remaining in water can induce the microorganisms and bacteria to generate resistance against the antibiotics, because of the selective pressure [4,5]. The World Health Organization has already issued a statement that the emergence as well as the diffusion of antibiotic-resistance bacteria (ARB) and antibiotic-resistance genes (ARGs) is posing threats to the public health security [6]. Although the ultra-violet (UV) and chlorination sterilization processes, which are widely applied in municipal wastewater treatment plants, possess good removal ability for the ARB, their ARGs removal effect are still far from

satisfactory [7]. In addition, the ozone oxidation process as well as the Fenton reaction also exhibits strong oxidation ability to some extents. However, the high energy consumption of the ozone oxidation and generated secondary contaminations in the Fenton reactions prohibit their broader applications [8–10]. Therefore, it is urgent to develop green and sustainable strategies for the efficient removal of the ARB and ARGs.

Recently, photocatalysis has gained considerable interests in sterilizations, due to its eco-friendliness and lack of secondary contaminations [11,12]. Researchers have pioneered the implementation of photocatalytic oxidation in effectively removing ARB among environments [13–15]. For instance, Chen et al. synthesized a plasmonic Z-scheme Ag@AgCl/PDI photocatalyst for the removal of ARB and ARGs [16], realizing completely removal of ARB in water within 2 hours, while the elimination of ARGs was limited. The activity was attributed to the

* Corresponding author at: State Key Laboratory of Environment-friendly Energy Materials, Southwest University of Science and Technology, Mianyang, Sichuan 621010, China.

E-mail address: quentin_xiong@swust.edu.cn (K. Xiong).

enhanced bacterial lysis by photocatalytic oxidation, thereby facilitating the diffusion of a significant number of extracellular resistance genes (e-ARGs). However, the short lifetime of reactive species (RSs) prevents effective destruction of remote e-ARGs from active sites, which those undamaged e-ARGs remain infectious and reproductive via horizontal gene transfer (HGT) [17–19]. Consequently, the pathway integrates with other bacteria, making them resistant to antibiotics [20]. Therefore, it is of great research importance to design photocatalyst that can confine e-ARGs within the reactive range of RSs. Generally, the external structure of DNA molecules is composed of pentose sugar and phosphate groups connected [21]. Therefore, designing photocatalysts with preferential adsorption of phosphate groups can constrain e-ARGs within the active range of RSs. In recent years, layered double hydroxides (LDHs) have been considered as one of the most effective photocatalysts for pollutant degradation, due to their elemental tunability, adsorption capability, and semiconductor properties [22–24].

Herein, zirconium-doped zinc-aluminum LDHs (Zn-Al-Zr LDHs) nanocomposites were successfully prepared, where metal cations (Al^{3+} , Zr^{4+}) with higher metal phosphate solubility product constants (pK_{sp}) and Zn^{2+} with selective adsorption of proteins were used as metal skeleton for the LDHs [25–27]. As a result, the synthesized Zn-Al-Zr LDHs managed to constraint ARB and ARGs within their nano-scaled texture and thereby shortened the space-time distance between RSs and ARB/ARGs, which was recognized as a special nano-confinement effect. Commonly, it exhibits enhanced catalytic efficiency when the reaction occurs in a limited space at the nanoscale, which is known as the Nano-confinement effect [28]. However, we did not use a limited nanoscale space to restrain the ARG molecule movements in this study. Our previous study have confirmed that the Zn-Al-Zr LDHs/GO nanocomposite has strong adsorption ability to the inorganic phosphate groups and organophosphorus molecules, whereas the outer skeleton of the DNA molecule consists of the phosphate ions and pentose molecules, so we utilize the strong ARG adsorption ability of the Zn-Al-Zr LDHs/GO nanocomposite to make the ARG molecules stay in the effective action radius, which differs from the well-recognized nano-confinement effect, it is a special nano-confinement effect [29]. Moreover, the separation efficiency of photogenerated carriers was further promoted by in-situ self-assembly on graphene oxide (GO) plane to synthesize the Zn-Al-Zr LDHs/GO nanocomposites [30,31]. At the same time, the photocatalytic performance of the Zn-Al-Zr LDHs/GO was verified through the removal experiments of ARB and ARGs. Furthermore, the inactivation and stress response mechanisms of ARB and ARGs during photocatalytic oxidation were investigated by label-free quantitative proteomics. The findings provide new insights into controlling the spread of antibiotic resistance in aquatic environments.

2. Materials and reagents

2.1. Materials and photocatalyst synthesis

The Zn-Al-Zr LDHs/GO was successfully synthesized through a straightforward co-precipitation method, with the GO preparation process detailed in our prior research [32]. Specifically, a mixed aqueous solution was prepared by dissolving ZnCl_2 , $\text{AlCl}_3 \cdot 6\text{H}_2\text{O}$, and $\text{ZrOCl}_2 \cdot 8\text{H}_2\text{O}$ with a molar mass ratio of 15:4:1 into 25 mL of deionized water, marked as Solution A. Meanwhile, an alkaline solution containing $\text{Na}_2\text{CO}_3 \cdot \text{H}_2\text{O}$ (0.1 M) and NaOH (0.4 M) was prepared, labelled as Solution B. The GO (5 mg) was dispersed ultrasonically in 20 mL of deionized water for 10 minutes. Following that, the solution A and B were added dropwise to the GO suspension under magnetic stirring with 150 rpm/min. The solution B was kept introducing until the pH value reached about 10. Then, the precipitation of LDH was allowed to be conducted for 12 hours at 90°C. Finally, the grey precipitates were filtered and rinsed with deionized water for 3 times and dried overnight at 90°C, harvesting the Zn-Al-Zr LDHs/GO nanocomposites.

Similarly, the preparation process of the Zn-Al-Zr LDHs was as

follows: the solution B were added dropwise to the solution A under magnetic stirring with 150 rpm/min. The subsequent process was consistent with the preparation process of the Zn-Al-Zr LDHs/GO.

2.2. The photocatalysis experiments of the Zn-Al-Zr LDHs/GO

Escherichia coli with a kanamycin resistance gene (*E. coli* (KanR)) was used as the ARB model. The removal performance of ARB was evaluated in a multi-tube agitated reactor (PCX50B, Beijing Perfect Light) under full-wavelength light irradiation (intensity: 70–100 mW/cm²). Specifically, 10 mg of the Zn-Al-Zr LDHs/GO and the prepared bacterial suspension were mixed in 50 mL of physiological saline and placed in a quartz flask, where the initial *E. coli* (KanR) concentration was $6.53 \log_{10}$ CFU/mL. The reaction mixture was stirred for 30 minutes in the dark to reach adsorption equilibrium. Subsequently, the light source was switched on to initiate the photocatalytic reaction. During the reaction processes, a certain quantity of reaction solution was periodically extracted and diluted by the physiological saline gradient to attain appropriate culture concentrations. Mixed cellulose filter membranes (47 mm with a pore size of 0.45 μm, PALL) were utilized for filtration and subsequently placed in petri dishes containing a culture medium of sodium dodecyl sulfate. The *E. coli* (KanR) concentration was determined using a plate counting method after incubation at 37°C for 24 hours. Meanwhile, the photocatalytic removal of ARGs was evaluated using pKMV plasmids with the kanamycin resistance genes (KanR genes) in the same to the *E. coli* (KanR) tests. Subsequently, the removal efficiency of the KanR genes should be precisely assessed using the quantitative polymerase chain reaction (qPCR) method. Details of the reaction procedure, primer sequence, and the qPCR standard curve are available in the Supporting Information (Table S1, Table S2, Figure S1 and Figure S2).

2.3. ARGs transformation assay

For the risk evaluation of the KanR genes horizontal transfer after photocatalytic treatments, 0.5 μL of the pKMV plasmids with different photocatalytic durations were mixed into 50 μL of *E. coli* DH5α. After 30 minutes under ice bathing, the mixture was swiftly transferred to a water bath of 42°C for 90 seconds to incorporate the plasmid into the *E. coli* DH5α. Then, 1 mL of LB liquid medium, as the essential nutrients required for bacterial growth, was dosed into the treated mixture. Subsequently, the above blended solution was then incubated in a continuous shaking incubator for an hour at 37°C to promote normal development. 100 μL of the above bacterial solution was then applied to a screening plate containing kanamycin. After incubating for 16–24 hours, the colonies growing on the plate were counted to assess the risk of ARGs spreading after photocatalytic treatments.

2.4. Reactive species (RSs) identification

The reactive oxygen species (ROS) generated by the Zn-Al-Zr LDHs/GO during photocatalytic oxidation were identified using an electron spin resonance spectrometer (ESR, EMXplus™, Bruker Biospin). Specifically, 2,2,6,6-Tetramethylpiperidinoxy (TEMPO) was utilized to capture singlet oxygen (${}^1\text{O}_2$) in water, while 5,5-dimethyl-1-pyrroline N-oxide (DMPO) was employed to capture hydroxyl radical ($\cdot\text{OH}$) in methanol and superoxide radical ($\cdot\text{O}_2^-$) in water, respectively. In addition, 1-hydroxy- 3-carboxy-2,2,5,5-tetramethylpyrrolidine (CPH) and 2,2,6,6-tetramethylpiperidine-1-oxyl (TEMPO) was used to capture the photogenerated hole (h^+) and photogenerated electrons (e^-) created by the Zn-Al-Zr LDHs/GO during photocatalysis, respectively [33]. To further elucidate the formation process and the corresponding contributions of free radicals in the photocatalysis, various scavengers were used to analyze the change of ARB concentrations. EDTA-Na₂ (1 mM), $\text{K}_2\text{Cr}_2\text{O}_7$ (0.5 mM), L-tryptophan (1 mM), and 4-Hydroxy-TEMPO (Tempol, 1 mM) scavengers were utilized for capturing h^+ , e^- , ${}^1\text{O}_2$,

and $\cdot\text{O}_2$, respectively [34]. At the same time, in order to further explore the role of O_2 , acetonitrile-d3 (CD_3CN , 10 mM) was also used in this study to extend the lifetime of O_2 [35].

2.5. Label-free quantitative proteomic analysis

Label-free quantitative proteomics technology was employed to analyze the protein content in ARB before and after photocatalytic reactions. This involved screening for differentially expressed proteins and bioinformatic analysis, aiming to thoroughly investigating the photocatalytic removal of ARB and the inactivation mechanism of ARGs. The *E. coli* (KanR) samples before and after the photocatalytic reaction were centrifuged for 5 minutes at 8000 rpm/min and 4°C to collect the *E. coli* (KanR). Subsequently, these samples were transferred into screw-capped tube. Finally, label-free quantitative experiments were conducted, following the reported protocols [36].

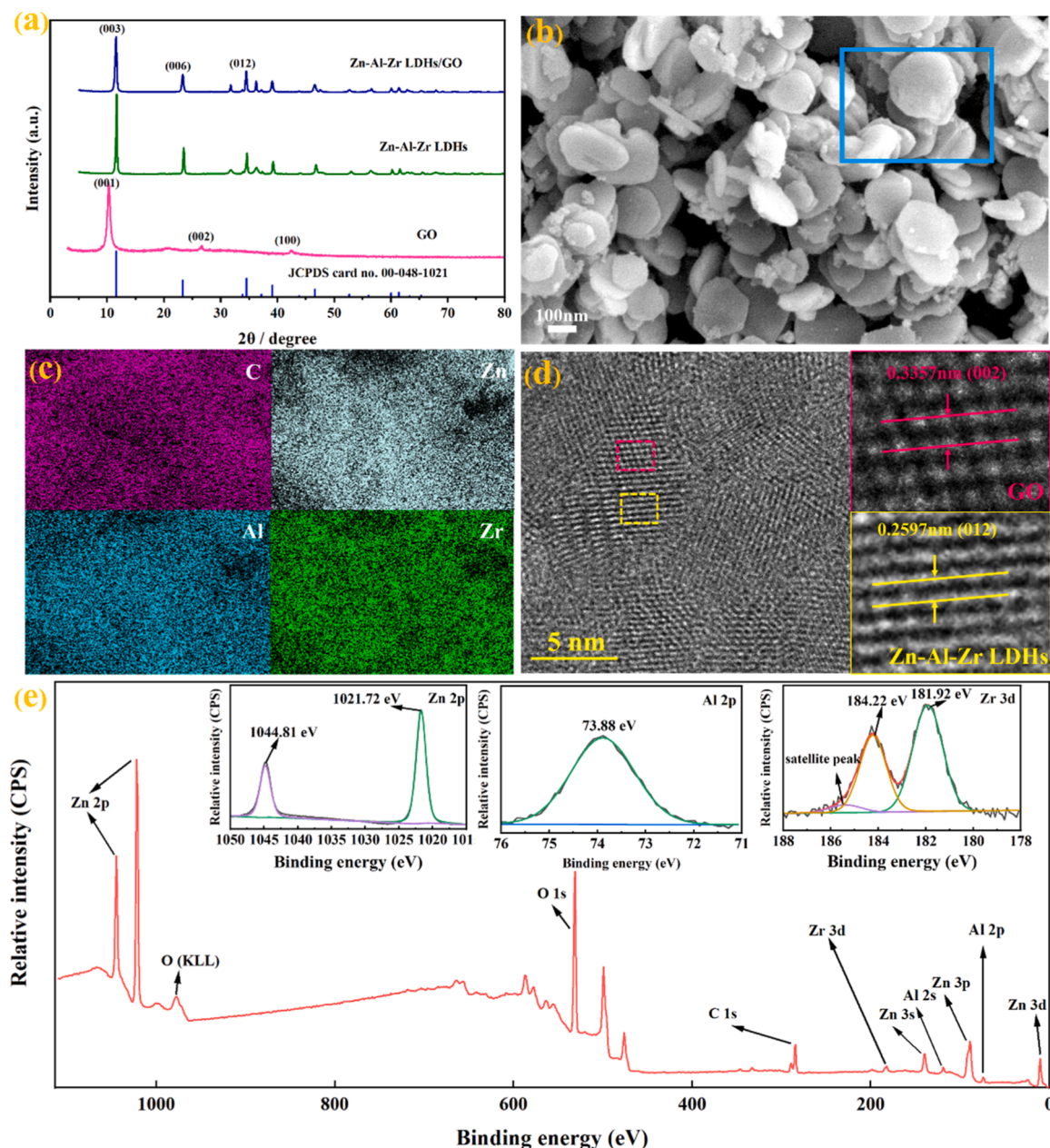


Fig. 1. (a) The XRD patterns of the GO, the Zn-Al-Zr LDHs, and the Zn-Al-Zr LDHs/GO. (b) SEM, (c) EDS mapping, (d) HRTEM of the samples. (e) XPS survey of the Zn-Al-Zr LDHs/GO, along with insets for high-resolution XPS spectra of Zn 2p, Al 2p and Zr 3d.

(Fig. 1c). Further, numerous nanosheet-like structure of the Zn-Al-Zr LDHs/GO composite was evidenced by TEM observations (Figure S3). Moreover, two kinds of distinct lattice stripes can be clearly identified in HRTEM images of the Zn-Al-Zr LDHs/GO (Fig. 1d), corresponding to the (002) lattice plane of the GO ($d=0.3359$ nm) and the characteristic (012) facets ($d=0.2597$ nm) of the Zn-Al-Zr LDHs, respectively.

As shown in Fig. 1e, the presence of C, Zn, Al, and Zr was further identified, in agreement with the EDS results. The uniform distribution of Zn^{2+} on the surface of the Zn-Al-Zr LDHs/GO was verified by the XPS peaks at 1021.72 eV ($Zn2p_{1/2}$) and 1044.81 eV ($Zn2p_{3/2}$). Additionally, the Al2p core level XPS spectrum showed a single peak at 73.88 eV attributed to the Al^{3+} species. The Zr3d core level XPS spectrum of the Zn-Al-Zr LDHs/GO revealed peaks at 181.92 eV and 184.22 eV, which were associated with $Zr3d_{5/2}$ and indicated the presence of Zr^{4+} species on the catalyst surface [37,38].

3.2. Recombination the photocatalyst with GO enhanced Photogenerated carrier separation and improving disinfection

Prior to activity evaluations, the dosage of the catalysts was optimized by assessing the photocatalytic removal efficiency of the *E. coli* (KanR) with varied catalysts additions. As a result, the optimal inactivation of the *E. coli* (KanR) with varied concentrations was all achieved at a dosage of 10 mg. Specifically, the *E. coli* (KanR) at concentrations of $7.42 \log_{10}$ CFU/mL, $6.53 \log_{10}$ CFU/mL and $5.56 \log_{10}$ CFU/mL were

completely removed within 60 minutes, 50 minutes and 40 minutes respectively (Fig. 2a, Figure S4). Therefore, the dosage of the samples was fixed to 10 mg in subsequent photocatalytic degradation experiments. To mimic conventional aqueous environments, the ARB concentrations of $6.53 \log_{10}$ CFU/mL was used in the study [39–41].

To preliminarily examine the photocatalytic properties, surface photovoltage (SPV) spectra were recorded for determining the efficiency of photogenerated carrier separation [42,43]. In contrast to the GO, both the Zn-Al-Zr LDHs and the Zn-Al-Zr LDHs/GO exhibited substantial SPV signal responses within the 300–400 nm (Fig. 2b). Besides, the SPV intensity of the Zn-Al-Zr LDHs/GO was 8.76 times higher than that of the Zn-Al-Zr LDHs. This may be due to GO serves as the electron enrichment center, which drives the photogenerated electrons to transfer from the Zn-Al-Zr LDHs to GO, so the Zn-Al-Zr LDHs/GO exhibits better photogenerated charge carrier separation ability than the Zn-Al-Zr LDHs [44,45]. Generally, the effective separation of the photogenerated carriers over the Zn-Al-Zr LDHs/GO composites would reflect the promising photocatalytic performance. Therefore, the inactivation performance of the *E. coli* (KanR) of the prepared samples was investigated. As expected, negligible photocatalytic decomposition of the *E. coli* (KanR) was observed over both the GO (with a decrease of $0.36 \log_{10}$ CFU/mL) and the blank control sample (with a decrease of $0.33 \log_{10}$ CFU/mL), ruling out the potential interference of GO and local condition. Strikingly, upon the introduction of the Zn-Al-Zr LDHs/GO, complete eradication of the *E. coli* (KanR) was rapidly reached within 60 minutes,

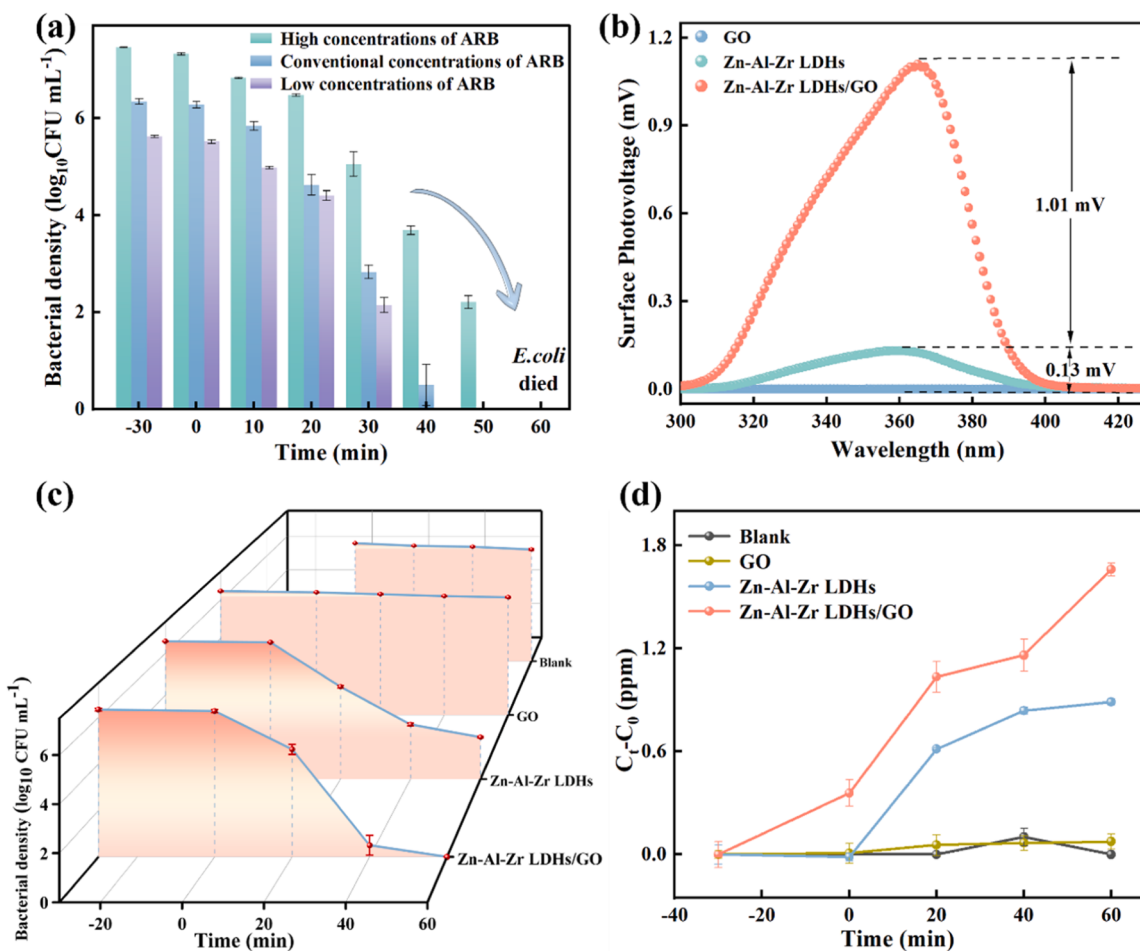


Fig. 2. (a) The performances of the Zn-Al-Zr LDHs/GO on photocatalytic inactivation of the *E. coli* (KanR) at three different initial concentrations of $5.56 \log_{10}$ CFU/mL, $6.53 \log_{10}$ CFU/mL and $7.42 \log_{10}$ CFU/mL, respectively; (b) the SPV spectra of the GO, Zn-Al-Zr LDHs and Zn-Al-Zr LDHs/GO; (c) the performances of the GO, Zn-Al-Zr LDHs and Zn-Al-Zr LDHs/GO on photocatalytic inactivation of the *E. coli* (KanR) with an initial concentration of $6.53 \log_{10}$ CFU/mL; (d) the concentrations of the K^+ in the solutions after the *E. coli* (KanR) with an initial concentration of $6.53 \log_{10}$ CFU/mL experienced the photocatalytic treatments by the GO, Zn-Al-Zr LDHs and Zn-Al-Zr LDHs/GO, respectively. The Blank group: the *E. coli* (KanR) was treated with the full-wavelength light irradiation in absence of photocatalyst.

while only $4.56 \log_{10}$ CFU/mL of the E. coli (KanR) was removed over the Zn-Al-Zr LDHs (Fig. 2c). The activity discrepancy could be assigned to the superior photogenerated carrier separation ability, echoing with the SPV results.

Furthermore, the removal rate of the E. coli (KanR) with the Zn-Al-Zr LDHs/GO was maintained above 99.99% even after five cycles (Figure S5). At the same time, the Zn-al-Zr LDHs/GO XPS spectra showed that the valence states of Zn, Al and Zr did not change significantly after 5 experimental cycles, demonstrating the exceptional stability of the Zn-Al-Zr LDHs/GO (Figure S6). Furthermore, to further verify the lipid oxidation in the cell membrane, the potassium ion (K^+) concentration in the photocatalytic reaction solution was measured by plasma optical emission spectrometer (ICP-OES, Thermo iCAP6500) to quantitatively determine the extent of cell membrane damage, which is in accordance with ARB death [46]. For the Zn-Al-Zr LDHs, there were 0.88 ppm of K^+ in the solution when after the E. coli (KanR) experienced its photocatalytic treatment for 60 minutes, whereas 1.66 ppm of K^+ were detected in the solution when the E. coli (KanR) underwent the photocatalytic treatment by the Zn-Al-Zr LDHs/GO for 60 minutes. The K^+ can diffuse from the intracellular into the solution only when cell membrane of E. coli (KanR) is broken. Therefore, it suggests that the Zn-Al-Zr LDHs/GO shows stronger ability to inactivate the E. coli (KanR). However, it almost had no effects on the inactivation the E. coli (KanR) after experiencing 60 minutes of photocatalytic treatments by the GO. Without the photocatalyst, it was also unable to inactivate the E. coli (KanR) only under the full-wavelength light irradiation (Fig. 2d).

3.3. Zn-Al-Zr LDHs/GO generated RSs and their contribution in photocatalytic disinfection

To obtain in-depth information of the photocatalytic procedures, ESR measurements were carried out to determine the generation of RSs by the Zn-Al-Zr LDHs/GO. As shown in Fig. 3a-e, the formation of h^+ , e^- ,

$\cdot O_2$, $\cdot O_2^-$ and $\cdot OH$ were obviously detected and their concentrations were accumulated with the prolonged exposure to light, while the ESR signals for $\cdot OH$ was absent. To further identify the specific contribution of the RSs including h^+ , e^- , $\cdot O_2$ and 1O_2 in photocatalytic process, EDTA-Na₂, K₂Cr₂O₇, Tempol and L-tryptophan scavengers were employed to capture individual RSs. Intriguingly, with the presence of EDTA-Na₂ (capturing h^+), the efficiency of deactivation for the E. coli (KanR) was significantly reduced to $1.05 \log_{10}$ CFU/mL of the E. coli (KanR), indicating the substantial involvement of h^+ in photo-sterilization (Fig. 3f). As a e^- scavenger, the addition of K₂Cr₂O₇ also resulted in a sluggish deactivation ($1.8 \log_{10}$ CFU/mL), implying a secondary role for e^- . Meanwhile, the E. coli (KanR) was reduced by only $3.41 \log_{10}$ CFU/mL within 60 minutes after L-tryptophan captured 1O_2 , demonstrating that 1O_2 was also an indispensable force in the photocatalytic sterilization process. Furthermore, as illustrated in Figure S7, when CD₃CN was added to prolong the survival time of 1O_2 , E. coli (KanR) was completely removed by the Zn-Al-Zr LDHs/GO within 30 min, while the control group required a longer time. This was another indication that 1O_2 played an important role in the photocatalytic disinfection of the Zn-Al-Zr LDHs/GO. Despite of the Tempol ($\cdot O_2^-$ scavenger) introduction, complete elimination of the E. coli (KanR) was still achieved within 60 minutes, excluding the direct contribution of $\cdot O_2^-$. The negligible involvement of $\cdot O_2^-$ during the photocatalysis could be caused by reactions with h^+ into 1O_2 free radicals [40]. Collectively, it is evident that h^+ and 1O_2 play pivotal roles in the Zn-Al-Zr LDHs/GO photoreaction system, and the mechanism was proposed accordingly: the photoexcited e^- and h^+ were separated over the Zn-Al-Zr LDHs/GO. Then, the e^- migrates to the GO, where dissolved oxygen is reduced into $\cdot O_2^-$ (1). Subsequently, the $\cdot O_2^-$ reacts with h^+ at the LDH, yielding 1O_2 (2).

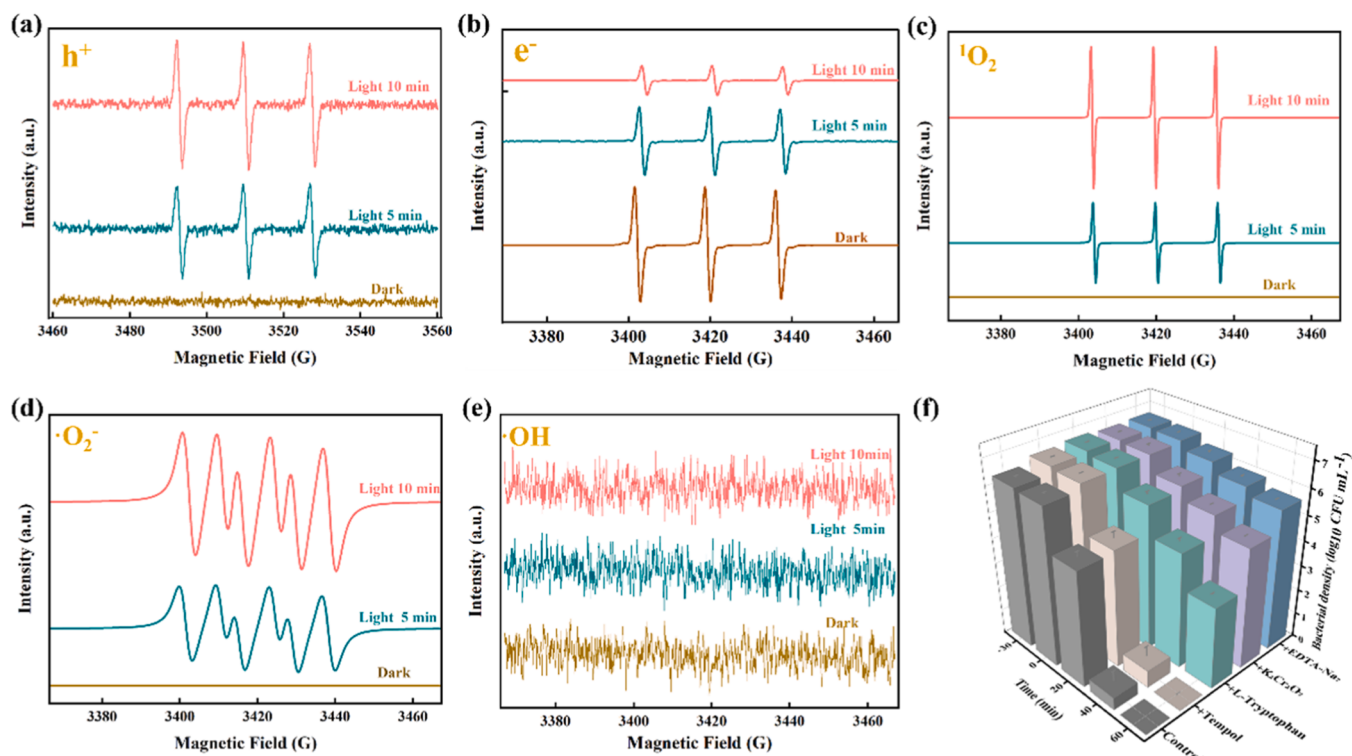
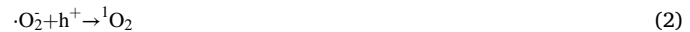


Fig. 3. (a) ESR spectrum obtained after h^+ was captured by CPH. (b) ESR spectrum obtained after e^- was captured by TEMPO. (c) ESR spectrum obtained after 1O_2 was captured by TEMP in aqueous medium. ESR spectra obtained after (d) $\cdot O_2^-$ in methanol medium (e) $\cdot OH$ in aqueous medium captured by DMPO. (f) The significance of different RSs in photocatalytic inactivation of the E. coli (KanR) was investigated by comparing with control group. h^+ , e^- , 1O_2 and $\cdot O_2^-$ were captured by EDTA-Na₂, K₂Cr₂O₇, L-tryptophan and Tempol, respectively.

3.4. Zn-Al-Zr LDHs/GO disrupted the *E. coli* (KanR) defense systems

To elucidate the stress response mechanism of the *E. coli* (KanR) during the photocatalytic reaction of the Zn-Al-Zr LDHs/GO, label-free quantitative proteomics was employed to assess the protein content of the *E. coli* (KanR) before and after photocatalytic treatments and bioinformatic analysis (Fig. 4). Figure S8 showed that the expression of key membrane proteins such as outer membrane protein A, outer membrane protein slp, outer membrane protein TolC and outer membrane protein assembly factor BamA was significantly downregulated after photocatalytic treatments, indicating a disturbance in the outer membrane integrity and normal function of the *E. coli* (KanR).

It is well-established that an insufficient supply of the energy molecule adenosine triphosphate (ATP) enhances the metabolic processes of glycolysis/gluconeogenesis [47,48]. In the photocatalytic treatment process, the dissolved oxygen in the water were almost transformed into $^1\text{O}_2$ and $\cdot\text{O}_2$, so actually the kanamycin-resistance (KanR) *E. coli* stay in the oxygen deficient environment at this time. Normally, the glycolysis/gluconeogenesis metabolic activities of the *E. coli* will be enhanced in the oxygen deficient environment, and the synthesis of the ATP is chiefly achieved through the substrate level phosphorylation process in this case. Under the aerobic condition, the ATP synthesis is usually accomplished by the oxidative phosphorylation process. In fact, the differential proteomic analysis results reveal that the oxidative phosphorylation process in the *E. coli* (KanR) is suppressed after they have experienced the photocatalytic treatment by the Zn-Al-Zr LDHs/GO (Figure S9). Meanwhile, the glycolysis/gluconeogenesis metabolic activity of the *E. coli* (KanR) was significantly increased (Figure S10). This was due to the upregulation of D-glucose phosphotransferase, aldolase, glyceraldehyde-3-phosphate dehydrogenase (phosphorylating), phosphoglycerate kinase, phosphoglycerate mutase, pyruvate kinase and alcohol dehydrogenase. Among them, D-glucose phosphotransferase and pyruvate kinase, as key enzymes involved in the irreversible reaction of glycolysis/ gluconeogenesis metabolism, enhanced the extra-cellular glucose utilization efficiency and pyruvate synthesis efficiency, respectively. Simultaneously, the expression of acetyl-CoA synthetase was downregulated, indicating a decrease in the conversion efficiency of pyruvate to acetyl-CoA. This would lead to a down-regulation of the citric acid cycle (Figure S11). Additionally, starch and sucrose

metabolism (Figure S12) were significantly down-regulated. The results suggest that photocatalytic treatments caused a significant decrease of ATP production in the *E. coli* (KanR), leading to the inhibition of essential life activities and the promotion of apoptosis in the *E. coli* (KanR). It could be attributed to prolonged oxidative stress in which $^1\text{O}_2$ interfered with the synthesis of NADH dehydrogenase, preventing the conversion of NADH to NAD⁺. It subsequently reduced the H⁺ transfer efficiency, thereby deteriorate ATP synthesis during oxidative phosphorylation (Fig. 5). Moreover, under oxidative stress, the expression of ATP synthase in the *E. coli* (KanR) was downregulated, further reducing ATP synthesis and accelerating bacterial death.

It is well known that the expression of genetic information requires the cooperation of various enzymes [49]. In this study, the significantly down-regulated expression of the DNA helicase in the KanR *E. coli* was due to the attack of the $^1\text{O}_2$ and the decreased ATP synthesis yield. As the chief energetic molecule in opening the DNA loop, the reduced yield of the ATP inevitably will lead to an impaired DNA replication process afterward. Since the DNA loop opening is prior to the DNA polymerization, it can clearly explain why the KanR *E. coli* exhibit down-regulated expressions of the DNA ligase and DNA polymerase after they have experienced the photocatalytic treatment for 30 min. In fact, some DNA repair proteins, such as the DNA repair protein (RadA) and the DNA mismatch repair proteins (MutS, MutL), all their expressions were completely inhibited. Therefore, it suggests that the integrity of the KanR *E. coli* and KanR gene suffer from the irreversible damages after the photocatalytic treatments by the Zn-Al-Zr LDHs/GO (Figure S13). Furthermore, exposure to $^1\text{O}_2$ increased the degradation efficiency of RNA in the *E. coli* (KanR), preventing normal genetic information expression (Figure S14). As a result, when the Zn-Al-Zr LDHs/GO adheres to the surface of the *E. coli* (KanR), RSs directly attacked its cell membrane, breaking the respiratory chain. RSs would then obstruct H⁺ transfer and ATP synthesis, significantly impacting all energy-dependent bacterial activities. The reduction in ATP and the oxidative stress state downregulate enzymes were crucial for genetic material replications and transcriptions, hindering normal genetic material expression.

It worth nothing to point out that ARGs share the very similar structures with DNA, thus the Zn-Al-Zr LDHs/GO would be promising in controlling the spread of ARGs through photocatalysis.

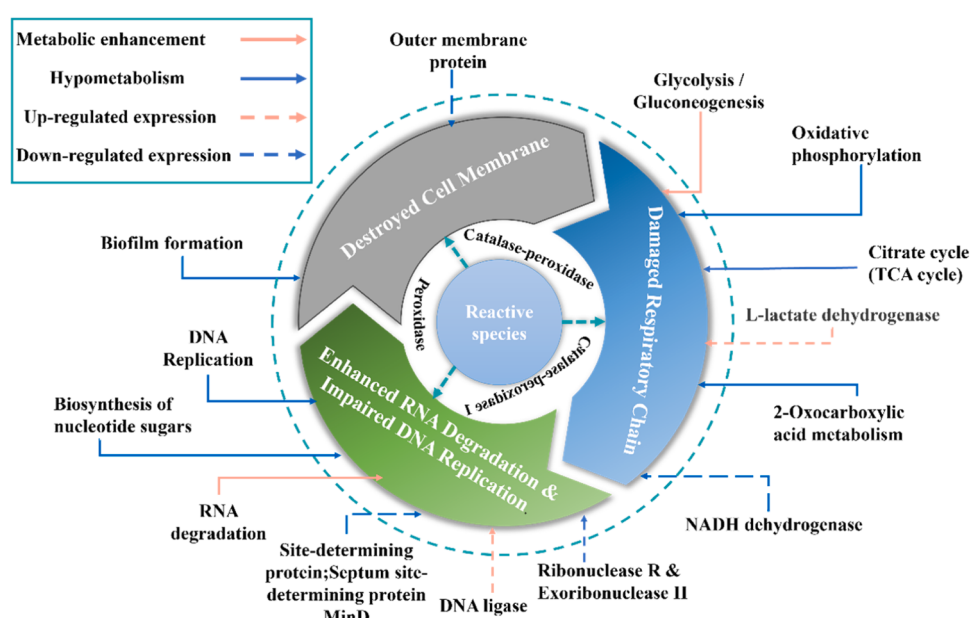


Fig. 4. Mechanism of ARB stress response during photocatalytic treatment.

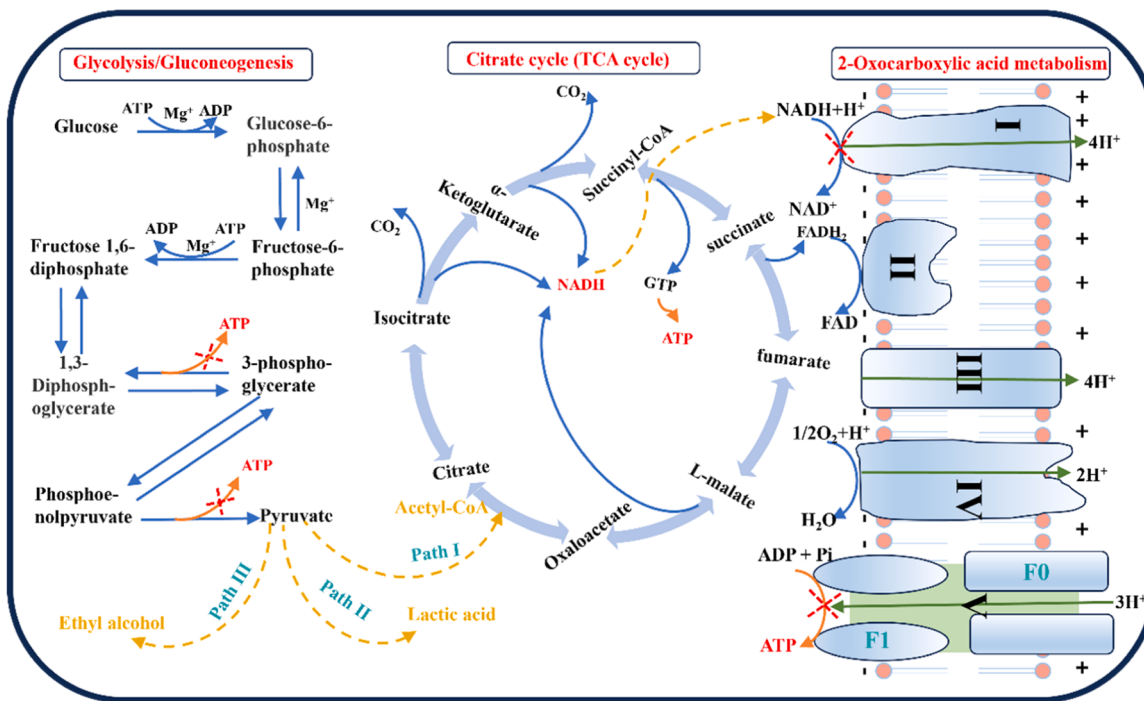


Fig. 5. Schematic diagram for the respiratory process of *E. coli* (KanR).

3.5. Zn-Al-Zr LDHs/GO enhanced photocatalytic removal ARGs

As proof-of-concept, the efficacy of the synthesized photocatalysts was systematically evaluated in the elimination of KanR e-ARGs. As a result, the concentration of the KanR genes in the reaction solution

containing the Zn-Al-Zr LDHs/GO decreased by $1.06 \log_{10}$ Copies/mL within 3 hours without illumination, exceeding that of the Zn-Al-Zr LDHs ($0.21 \log_{10}$ Copies/mL) and the GO ($0.17 \log_{10}$ Copies/mL). The overwhelming adsorption ability of the Zn-Al-Zr LDHs/GO could be contributed to the superior affinity of the KanR genes (Fig. 6a). As shown

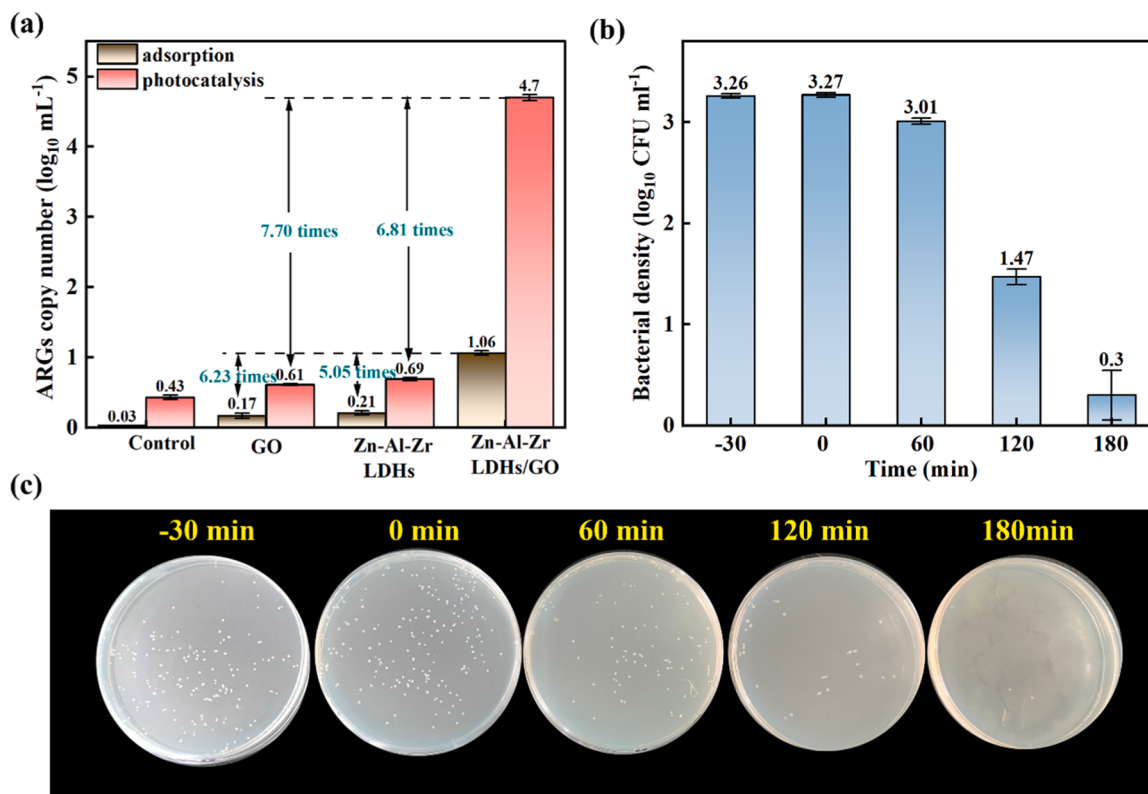


Fig. 6. (a) The removal efficiency of the KanR genes after dark adsorption and light reaction 3 hours. (b) A transformation experiment was conducted to assess residual the KanR genes after the Zn-Al-Zr LDHs/GO photoreaction, and (c) colony growth on screening medium (kanamycin) was analyzed.

in Table S3, the zeta potential of the Zn-Al-Zr LDHs/GO and the Zn-Al-Zr LDHs were 14.2 mV and 6.37 mV, respectively. However the zeta potential of the KanR genes were -3.38 mV, indicating that the Zn-Al-Zr LDHs/GO was more favorable for the adsorption of the KanR gene. In addition, the specific surface area of the Zn-Al-Zr LDHs/GO was $70.92 \text{ m}^2/\text{g}$, whereas that of the Zn-Al-Zr LDHs was $55.47 \text{ m}^2/\text{g}$, implying that the Zn-Al-Zr LDHs/GO also has a larger specific surface area than the Zn-Al-Zr LDHs (Figure S15). Therefore, the more positive charge and larger specific surface area endow the Zn-Al-Zr LDHs/GO with stronger KanR gene adsorption ability in comparison with the Zn-Al-Zr LDH. This was helpful to shorten the distance between the KanR genes and the active site in the photocatalytic reaction and improve the removal efficiency of the KanR genes.

In fact, when exposing the systems to light, the concentration of the KanR genes in the Zn-Al-Zr LDHs/GO-containing solution was decreased to $4.70 \log_{10}$ copies/mL within 3 hours, which were 6.81 times higher than that of the Zn-Al-Zr LDHs. Given that the high photocatalytic inactivation and strong adsorption capability of the KanR genes, the Zn-Al-Zr LDHs/GO immobilized the ARGs via a nano-confinement effect and ensured their decomposition by the singlet oxygen (Fig. 6a). This was due to the fact that Zn-Al-Zr LDHs/GO not only has high photocatalytic performance, but can also bind the KanR genes through the special nano-confinement effects to achieve efficient removal of the KanR gene.

It should be noted that the photocatalytic removal of ARGs is influenced by various factors, including gene length, host cell type, operating conditions, and light source. Long gene sequences have more targets in the photocatalytic oxidation process than short gene sequences [39]. The length of the KanR genes is shorter than that of ampC and tetM, making it more difficult to remove. Additionally, sublethal damage of e-ARGs can be repaired when they enter host cells [50].

Therefore, to investigate the potential dissemination of the residual KanR genes after photocatalytic treatments, these transformation and regrowth capabilities of the genes were correspondingly assessed (Fig. 6b and c). A significant decrease in the number of bacteria on the selective medium was witnessed as the illumination duration increased. At -30 min, the infection level of the KanR genes was $3.26 \log_{10}$ copies/mL. After illuminated for 3 hours, the infection level was dropped to $0.3 \log_{10}$ CFU/mL, demonstrating the RSs created by the Zn-Al-Zr LDHs/GO destroyed the KanR genes at molecular level. Thus, the spread antibiotic resistance could be substantially suppressed.

4. Conclusion

In conclusion, a Zn-Al-Zr LDHs/GO nanocomposite material was successfully developed using a facile co-precipitation method. The Zn-Al-Zr LDHs/GO was used as an active photocatalyst to construct a nano-confinement photocatalytic system for the efficient removal of ARB and ARGs. The unique nano-confinement effects of Zn-Al-Zr LDHs/GO, compared to conventional nano-confinement effects, was achieved by the adsorption of phosphoric acid molecules, which can avoid the interference of background components and improve the removal efficiency of ARB and ARGs. The prepared Zn-Al-Zr LDHs/GO was capable of photocatalysis eradicating various concentrations of the *E. coli* (KanR) ($5.56 \log_{10}$ CFU/mL, $6.53 \log_{10}$ CFU/mL, $7.42 \log_{10}$ CFU/mL) within 60 minutes. Moreover, leveraging the combined effects of photocatalysis and nano-confinement, the KanR genes removal can be achieved up to $4.70 \log_{10}$ copies/mL within 3 hours. Besides, the experiments of free radical capture and differential protein analysis revealed that the photogenerated ${}^1\text{O}_2$ could disrupt the ARB oxidation respiratory chain, significantly diminishing ATP production and hastening ARB mortality. Furthermore, the formation of ${}^1\text{O}_2$ also led to decreased expressions of multiple enzyme proteins in the *E. coli* (KanR), effectively impeding the dissemination of the KanR genes. Collectively, the present work offers a novel approach for sterilizing ARB and ARGs by photocatalytic routes.

CRediT authorship contribution statement

Dawei Liu: Data curation. **Miao Yu:** Writing – original draft, Validation, Investigation, Formal analysis, Data curation. **Kun Xiong:** Writing – review & editing, Supervision, Resources, Project administration, Conceptualization. **Jun Wang:** Supervision, Resources, Project administration. **Xiaofeng Zhu:** Writing – review & editing, Visualization. **Yuqiu Fan:** Investigation, Data curation. **Jianhui Ren:** Software, Methodology. **Jing Xia:** Resources. **Lichao Wang:** Resources, Conceptualization.

Declaration of Competing Interest

No conflict of interest exists in the submission of this manuscript, and manuscript is approved by all authors for publication. I would like to declare on behalf of my co-authors that the work described was original research that has not been previously published, and not under consideration for publication elsewhere, in whole or in part. All the authors listed have approved the manuscript that is enclosed. I also declare that it will not be published elsewhere in the same form, in English or in any other language, without the written consent of the Publisher after acceptance.

Data Availability

Data will be made available on request.

Acknowledgements

This work is financially supported by the National Natural Science Foundation of China (no. 21906132, no. 22176155), Sichuan Science and Technology Program (Grant no. 2021YJ0317), Longshan academic talent research supporting program of SWUST (no. 18LZX533).

Appendix A. Supporting information

Supplementary data associated with this article can be found in the online version at doi:10.1016/j.apcatb.2024.123922.

References

- [1] Y. Ben, C. Fu, M. Hu, L. Liu, M.H. Wong, C. Zheng, Human health risk assessment of antibiotic resistance associated with antibiotic residues in the environment: A review, Environ. Res. 169 (2019) 483–493.
- [2] J. Liu, J. Wu, C. Zhang, Y. Zhang, Y. Lin, Y. Luo, Occurrence, distribution, and ecological-health risks of selected antibiotics in coastal waters along the coastline of China, Sci. Total Environ. 644 (2018) 1469–1476.
- [3] B. Shao, Z. Liu, L. Tang, Y. Liu, Q. Liang, T. Wu, Y. Pan, X. Zhang, X. Tan, J. Yu, The effects of biochar on antibiotic resistance genes (ARGs) removal during different environmental governance processes: A review, J. Hazard. Mater. 435 () (2022).
- [4] N. Kurt Yilmaz, C.A. Schiffer, Introduction: Drug Resistance, Chem. Rev. 121 (2021) 3235–3237.
- [5] H. Yin, G. Li, X. Chen, W. Wang, P.K. Wong, H. Zhao, T. An, Accel. Evol. Bact. Antibiot. Resist. Early emerged Stress Responses driven Photo Oxid., Appl. Catal. B: Environ. 269 (2020) 118829.
- [6] <GLOBAL Action plan on antimicrobial resistance.pdf>.
- [7] S. Phattarapattamawong, N. Charuewan, C. Polprasert, Comparative removal of two antibiotic resistant bacteria and genes by the simultaneous use of chlorine and UV irradiation (UV/chlorine): Influence of free radicals on gene degradation, Sci. Total Environ. 755 (2021) 142696.
- [8] M. Foroughi, M. Khadiani, S. Kakhki, V. Kholghi, K. Naderi, S. Yektay, Effect of ozonation-based disinfection methods on the removal of antibiotic resistant bacteria and resistance genes (ARB/ARGs) in water and wastewater treatment: a systematic review, Sci. Total Environ. 811 (2022) 151404.
- [9] Y. Ahmed, J. Lu, Z. Yuan, P.L. Bond, J. Guo, Efficient inactivation of antibiotic resistant bacteria and antibiotic resistance genes by photo-Fenton process under visible LED light and neutral pH, Water Res. 179 (2020).
- [10] Y. Ahmed, J. Zhong, Z. Wang, L. Wang, Z. Yuan, J. Guo, Simultaneous removal of antibiotic resistant bacteria, antibiotic resistance genes, and micropollutants by FeS2@GO-based heterogeneous photo-fenton process, Environ. Sci. Technol. 56 (2022) 15156–15166.

- [11] K.K. Gangu, S. Maddila, S.B. Jonnalagadda, A review on novel composites of MWCNTs mediated semiconducting materials as photocatalysts in water treatment, *Sci. Total Environ.* 646 (2019) 1398–1412.
- [12] S.K. Loeb, P.J.J. Alvarez, J.A. Brame, E.L. Cates, W. Choi, J. Crittenden, D. D. Dionysiou, Q. Li, G. Li-Puma, X. Quan, D.L. Sedlak, T. David Waite, P. Westerhoff, J.-H. Kim, The technology horizon for photocatalytic water treatment: sunrise or sunset? *Environ. Sci. Technol.* 53 (2019) 2937–2947.
- [13] J. Zhong, Y. Ahmed, G. Carvalho, Z. Wang, L. Wang, J.F. Mueller, J. Guo, Simultaneous removal of micropollutants, antibiotic resistant bacteria, and antibiotic resistance genes using graphitic carbon nitride under simulated solar irradiation, *Chem. Eng. J.* 433 (2022) 133839.
- [14] N.K. Eswar, S.A. Singh, G. Madras, Photoconductive network structured copper oxide for simultaneous photoelectrocatalytic degradation of antibiotic (tetracycline) and bacteria (*E. coli*), *Chem. Eng. J.* 332 (2018) 757–774.
- [15] H. Yin, X. Chen, G. Li, W. Wang, P.K. Wong, T. An, Can photocatalytic technology facilitate conjugative transfer of ARGs in bacteria at the interface of natural sphalerite under different light irradiation? *Appl. Catal. B: Environ.* 287 (2021).
- [16] X. Chen, Z. Wang, X. Shen, Y. Zhang, Y. Lou, C. Pan, Y. Zhu, J. Xu, A plasmonic Z-scheme Ag@AgCl/PDI photocatalyst for the efficient elimination of organic pollutants, antibiotic resistant bacteria and antibiotic resistance genes, *Appl. Catal. B: Environ.* 324 (2023) 122220.
- [17] S. Li, C. Zhang, F. Li, T. Hua, Q. Zhou, S.-H. Ho, Technologies towards antibiotic resistance genes (ARGs) removal from aquatic environment: a critical review, *J. Hazard. Mater.* (411) 0 (2021).
- [18] M.-A. Nnorom, D. Saroj, L. Avery, R. Hough, B. Guo, A review of the impact of conductive materials on antibiotic resistance genes during the anaerobic digestion of sewage sludge and animal manure, *J. Hazard. Mater.* 446 (2023) 130628.
- [19] Z. Wei, K. Feng, Z. Wang, Y. Zhang, M. Yang, Y.-G. Zhu, M.P.J. Virta, Y. Deng, High-Throughput Single-Cell Technology Reveals the Contribution of Horizontal Gene Transfer to Typical Antibiotic Resistance Gene Dissemination in Wastewater Treatment Plants, *Environ. Sci. Technol.* 55 (2021) 11824–11834.
- [20] Y. Chen, P. Li, Y. Huang, K. Yu, H. Chen, K. Cui, Q. Huang, J. Zhang, K. Yew-Hoong Gin, Y. He, Environmental media exert a bottleneck in driving the dynamics of antibiotic resistance genes in modern aquatic environment, *Water Res.* 162 (2019) 127–138.
- [21] Q. Li, Z. Tong, Y. Cao, H. Gu, DNAs catalyzing DNA nanoconstruction, *Chem* 7 (2021) 2556–2568.
- [22] J. Yang, C. Li, D. Liang, Y. Liu, Z. Li, H. Wang, H. Huang, C. Xia, H. Zhao, Y. Liu, Q. Zhang, Z. Meng, Central-collapsed structure of CoFeAl layered double hydroxides and its photocatalytic performance, *J. Colloid Interface Sci.* 590 (2021) 571–579.
- [23] G. Zhang, X. Zhang, Y. Meng, G. Pan, Z. Ni, S. Xia, Layered double hydroxides-based photocatalysts and visible-light driven photodegradation of organic pollutants: a review, *Chem. Eng. J.* 392 (2020) 123684.
- [24] R. Pelalak, A. Hassani, Z. Heidari, M. Zhou, State-of-the-art recent applications of layered double hydroxides (LDHs) material in Fenton-based oxidation processes for water and wastewater treatment, *Chem. Eng. J.* 474 (2023) 145511.
- [25] J.L. Milagres, C.R. Bellato, R.S. Vieira, S.O. Ferreira, C. Reis, Preparation and evaluation of the Ca-Al layered double hydroxide for removal of copper(II), nickel (II), zinc(II), chromium(VI) and phosphate from aqueous solutions, *J. Environ. Chem. Eng.* 5 (2017) 5469–5480.
- [26] F. Tang, H. Yang, H. Chen, M. Zhou, P. Huang, Y. He, P. Song, R. Wang, Preparation of ZrLDH-based 3D microspheres for phosphate recovery, *J. Environ. Chem. Eng.* 10 (2022) 108484.
- [27] T.S. Choi, F.A. Tezcan, Design of a flexible, Zn-selective protein scaffold that displays anti-irving-williams behavior, *J. Am. Chem. Soc.* 144 (2022) 18090–18100.
- [28] B. Dong, Y. Pei, N. Mansour, X. Lu, K. Yang, W. Huang, N. Fang, Deciphering nanoconfinement effects on molecular orientation and reaction intermediate by single molecule imaging, *Nat. Commun.* 10 (2019).
- [29] J. Ren, Y.-Y. Huang, D. Li, M. Yu, L. Chen, J. Wang, K. Xiong, Tremella-like Zn-Al-Zr-layered double-hydroxide/graphene oxide nanocomposites for enhanced phosphorus recovery, *ACS Appl. Nano Mater.* 7 (2024) 2143–2154.
- [30] H. Yan, Y.-H. Liu, Y. Yang, H.-Y. Zhang, X.-R. Liu, J.-Z. Wei, L.-L. Bai, Y. Wang, F.-M. Zhang, Covalent organic framework based WO₃@COF/rGO for efficient visible-light-driven H₂ evolution by two-step separation mode, *Chem. Eng. J.* 431 (2022) 133404.
- [31] D. Li, P. Yu, X. Zhou, J.-H. Kim, Y. Zhang, P.J.J. Alvarez, Hierarchical Bi₂O₂CO₃ wrapped with modified graphene oxide for adsorption-enhanced photocatalytic inactivation of antibiotic resistant bacteria and resistance genes, *Water Res.* 184 (2020).
- [32] K. Xiong, Q. Fan, T. Wu, H. Shi, L. Chen, M. Yan, Enhanced bovine serum albumin absorption on the N-hydroxysuccinimide activated graphene oxide and its corresponding cell affinity, *Mater. Sci. Eng.: C* 81 (2017) 386–392.
- [33] H. Jia, W. He, W.G. Wamer, X. Han, B. Zhang, S. Zhang, Z. Zheng, Y. Xiang, J.-J. Yin, Generation of Reactive Oxygen Species, Electrons/Holes, and Photocatalytic Degradation of Rhodamine B by Photoexcited CdS and Ag₂S Micro-Nano Structures, *The, J. Phys. Chem. C* 118 (2014) 21447–21456.
- [34] W. Deng, K. Xiong, N. Ge, M. Yu, L. Chen, J. Wang, Cobalt and titanium co-doped zinc ferrite film photoanode with boosted interfacial photoelectrocatalytic activity for efficient degradation of tetracycline via the covalency competition in the Zn-O-Fe backbone, *Chem. Eng. J.* 433 (2022).
- [35] K. Xiong, Y. Wang, F. Zhang, X. Li, X. Lang, Linker length-dependent photocatalytic activity of β -ketoenamine covalent organic frameworks, *Appl. Catal. B: Environ.* 322 (2023) 122135.
- [36] S.-P. Yang, J. Xie, Y. Cheng, Z. Zhang, Y. Zhao, Y.-F. Qian, Response of *Shewanella putrefaciens* to low temperature regulated by membrane fluidity and fatty acid metabolism, *Lwt* 117 (2020).
- [37] J. Zhang, T. Yan, Y. Yang, J. Sun, Y. Lin, M. Wei, Zn-Zr-Al oxides derived from hydrotalcite precursors for ethanol conversion to diethyl carbonate, *Chin. J. Catal.* 40 (2019) 515–522.
- [38] S. Hu, K. J.-n. Gu, J. Li, Y. Liang, X. Xue, M. Min, X. Guo, J. Hu, T. Jia, Sun, Boosting COS catalytic hydrolysis performance over Zn-Al oxide derived from ZnAl hydrotalcite-like compound modified via the dopant of rare earth metals and the replacement of precipitation base, *Appl. Surf. Sci.* 599 (2022) 154016.
- [39] X. Chen, W. Han, M. Patel, Q. Wang, Q. Li, S. Zhao, W. Jia, Inactivation of a pathogenic NDM-1-positive *Escherichia coli* strain and the resistance gene blaNDM-1 by TiO₂/UVA photocatalysis, *Sci. Total Environ.* 846 (2022).
- [40] C.B. Özkal, D. Venieri, I. Gounaki, S. Meric, Assessment of thin-film photocatalysis inactivation of different bacterial indicators and effect on their antibiotic resistance profile, *Appl. Catal. B: Environ.* 244 (2019) 612–619.
- [41] C. Guo, K. Wang, S. Hou, L. Wan, J. Lv, Y. Zhang, X. Qu, S. Chen, J. Xu, H₂O₂ and/or TiO₂ photocatalysis under UV irradiation for the removal of antibiotic resistant bacteria and their antibiotic resistance genes, *J. Hazard. Mater.* 323 (2017) 710–718.
- [42] Y. Zhu, W. Deng, L. Chen, J. Courtois, Q. Tian, X. Zhang, L. Almásy, M. Yan, K. Xiong, Langmuir-Blodgett-assembled monolayer zinc ferrite nanoparticle film with unique photogenerated charge carrier separation efficiency and charge transfer behavior, *Appl. Surf. Sci.* 534 (2020).
- [43] R. Chen, F. Fan, T. Dittrich, C. Li, Imaging photogenerated charge carriers on surfaces and interfaces of photocatalysts with surface photovoltage microscopy, *Chem. Soc. Rev.* 47 (2018) 8238–8262.
- [44] Y. Gong, B. Yang, H. Zhang, X. Zhao, C. Zhu, Graphene oxide enwrapped polyimide composites with efficient photocatalytic activity for 2,4-dichlorophenol degradation under visible light irradiation, *Mater. Res. Bull.* 112 (2019) 115–123.
- [45] H. Yan, Y.-H. Liu, Y. Yang, H.-Y. Zhang, X.-R. Liu, J.-Z. Wei, L.-L. Bai, Y. Wang, F.-M. Zhang, Covalent organic framework based WO₃@COF/rGO for efficient visible-light-driven H₂ evolution by two-step separation mode, *Chem. Eng. J.* 431 (2022).
- [46] M.A. Quinteros, V. Cano Aristizábal, P.R. Dalmasso, M.G. Paraje, P.L. Pérez, Oxidative stress generation of silver nanoparticles in three bacterial genera and its relationship with the antimicrobial activity, *Toxicol. Vitr.* 36 (2016) 216–223.
- [47] X.-I. Bian, H.-z. Chen, P.-b. Yang, Y.-p. Li, F.-n. Zhang, J.-y. Zhang, W.-j. Wang, W.-x. Zhao, S. Zhang, Q.-t. Chen, Y. Zheng, X.-y. Sun, X.-m. Wang, K.-Y. Chien, Q. Wu, Nur77 suppresses hepatocellular carcinoma via switching glucose metabolism toward gluconeogenesis through attenuating phosphoenolpyruvate carboxykinase sumoylation, *Nature Communications* 8 (2017) 14420.
- [48] C.-S. Zhang, S.A. Hawley, Y. Zong, M. Li, Z. Wang, A. Gray, T. Ma, J. Cui, J.-W. Feng, M. Zhu, Y.-Q. Wu, T.Y. Li, Z. Ye, S.-Y. Lin, H. Yin, H.-L. Piao, D.G. Hardie, S.-C. Lin, Fructose-1,6-bisphosphate and aldolase mediate glucose sensing by AMPK, *Nature* 548 (2017) 112–116.
- [49] C.-Y. Lo, Y. Gao, DNA helicase–polymerase coupling in bacteriophage DNA replication, *Viruses* 13 (2021).
- [50] P.H. Chang, B. Juhrerd, T.M. Olson, C.F. Marrs, K.R. Wigginton, degradation of extracellular antibiotic resistance genes with UV254 treatment, *Environ. Sci. Technol.* 51 (2017) 6185–6192.